Proceedings of the 11th Brazilian Congress of Thermal Sciences and Engineering -- ENCIT 2006
Braz. Soc. of Mechanical Sciences and Engineering -- ABCM, Curitiba, Brazil,- Dec. 5-8, 2006

Paper CIT06-0490

COMPRESSIBILITY EFFECT ON AERODYNAMIC HEATING AND DRAG OF HYPERSONIC FLOW OVER FLAT-NOSE LEADING EDGES

Wilson F. N. Santos
Combustion and Propulsion Laboratory
National Institute for Space Research
12630-000 Cachoeira Paulista, SP, Brazil
wilson@lcp.inpe.br

Abstract. *In designing rarefied hypersonic vehicles one fundamental problem that must be solved regards the aerodynamics of re-entry. This challenging problem is nowadays handled by using the Direct Simulation Monte Carlo (DSMC) method In this work, the hypersonic two-dimensional flow around a family of blunt leading edges at an altitude of 70 km is investigated by using the DSMC method. The effect of compressibility on the aerodynamic surface quantities is investigated for flat-nose leading edges. Numerical simulations were performed for freestream Mach numbers of 5, 8 and 12. The aerothermodynamic performance of the flat-nose leading edges is assessed by using the pressure, skin friction, heat transfer and total drag coefficients. The calculation results depict a weak effect of the leading-edge thickness on total drag, while predict a significant dependence of drag on the freestream Mach number over the range examined. The data generated in the present account is part of an investigation in order to determine and to quantify the benefits and disadvantages of using these new blunt shapes over circular cylinder shapes.*

Keywords. *DSMC, aerodynamic heating, hypersonic flow, rarefied flow, blunt leading edge.*

1. Introduction

Hypersonic vehicles experience severe aerothermodynamic heating during the atmospheric entry path. As a result, the design of a thermal protection system in order to protect the vehicles from the intense heat load is a critical task. The selection of material type depends on the surface temperature, which is determined from the local heat transfer rate. In addition, the nose radius or nose tip for hypersonic vehicles is determined so that the maximum surface temperature does not exceed the upper limit temperature of the material used for thermal protection system. Due mainly to improvements in the material used for thermal protection system, the radius of the leading edges or nose tips can be reduced significantly. Consequently, the wave drag is reduced and the aerodynamic efficiency is improved.

A method of designing low heat transfer bodies is devised on the premise that the rate of heat transfer to the nose will be low if the local velocity is low, while the rate of heat transfer to the afterbody will be low if the local density is low (Reller, 1957). A typical body that results from this design method consists of a flat nose followed by a highly curved, but for the most part slightly inclined, afterbody surface. Due mainly to manufacturing problems and the extremely high temperatures attained in hypersonic flight, flat-nose leading edges have been considered (Santos, 2003, 2004, and 2005) as especially promising bluntness for hypersonic configurations.

Santos (2003) has investigated the effect of the leading-edge thickness on the flowfield structure over these flat-nose leading edges. The thickness effect was examined for a range of Knudsen number, based on the thickness of the flat nose, covering from the transitional flow regime to the free molecular flow regime. The emphasis of the work was to compare the heat transfer and drag of these new flat-nose leading edges with those obtained for circular cylinder shape, typically assumed as the appropriate blunting geometry for heat transfer considerations. It was found that flat-nose leading edges provided much smaller drag than round leading edges. Nevertheless, round leading edge still presented smaller stagnation point heating than flat-nose leading edges for the conditions investigated. Nevertheless, flat-nose bodies have more volume than round leading edges. In this respect, the overall heat transfer to these leading edges may be tolerate if there is an active cooling, since additional coolant may be placed in the leading edge.

Santos (2004) has extended the analysis presented by Santos (2003) by performing a parametric study on these shapes with a great deal of emphasis placed on the wall temperature effects. In this scenario, the primary aim was to assess the sensitivity of the pressure, skin friction, heat transfer and drag coefficients to variations on the body surface temperature. Calculations showed that the heat transfer coefficient decreased with increasing the wall temperature. It was also found that the total drag slightly increased by increasing the wall temperature.

The works of Santos (2003 and 2004) have been concentrated primarily on the analysis of the flowfield structure by considering the diffuse reflection model as being the gas-surface interaction. Nonetheless, as a space flight vehicle is exposed to a rarefied environment over a considerable time, a departure from the fully diffuse model is observed, resulting from the colliding molecules that clean the surface of the vehicle, which becomes gradually decontaminated. In this scenario, Santos (2005) has performed a parametric study on these shapes with a great effort placed on the gas-surface interaction effects. The primary idea of the paper was to assess the sensitivity of the flowfield structure to variations on the surface accommodation coefficients experienced by the leading edges.

In order to provide information on how well these shapes stand up as possible candidates for blunting geometries of

hypersonic leading edges, the present account extends the analysis presented by Santos (2003, 2004 and 2005) by performing a parametric study on these shapes with a great deal of emphasis placed on the compressibility effects. In this connection, this study will objectively assess the sensitivity of the aerodynamic surface quantities, such as pressure, skin friction, heat transfer and drag coefficients, to variations on the freestream Mach number.

The study at hand focuses on the low-density region in the upper atmosphere. High-speed flows under low-density conditions deviate from a perfect gas behavior because of the excitation of rotation, vibration and possible dissociation. At high altitudes, and therefore, low density, the molecular collision rate is low and the energy exchange occurs under non-equilibrium conditions. In such a circumstance, the degree of molecular non-equilibrium is such that the Navier-Stokes equations are inappropriate. Therefore, the Direct Simulation Monte Carlo method will be employed to calculate the hypersonic two-dimensional flow on the leading edges.

2. Leading-Edge Configuration

In dimensionless form, the contour that defines the shape of the afterbody surface (Santos, 2003, 2004 and 2005) is as following,

$$\bar{x} = \int_{\bar{y}=1}^{\bar{y}=\bar{y}_{\max}} \sqrt{\bar{y}^{k} - 1}\, d\bar{y} \tag{1}$$

where $\bar{x} = x/y_{nose}$ and $\bar{y} = y/y_{nose}$.

The blunt shapes are modeled by assuming a sharp leading edge of half angle θ with a circular cylinder of radius R inscribed tangent to the wedge. The blunt shapes, inscribed between the wedge and the cylinder, are also tangent to them at the same common point where they have the same slope angle. It was assumed a leading edge half angle of 10 degrees, a circular cylinder diameter of 10^{-2}m and flat-nose thickness t/λ_∞ of 0.01, 0.1 and 1, where $t = 2y_{nose}$ and λ_∞ is the freestream mean free path. Figure (1a) illustrates this construction for the set of shapes investigated. From geometric considerations, the exponent k in Eq. (1) is obtained by matching slope on the wedge, circular cylinder and on the body shapes at the tangency point. For dimensionless thickness t/λ_∞ of 0.01, 0.1 and 1, the exponent k corresponds to 0.501, 0.746 and 1.465, respectively. The common body height H and the body length L are obtained in a straightforward manner. It was assumed that the leading edges are infinitely long but only the length L is considered, since the wake region behind the leading edges is not of interest in this investigation.

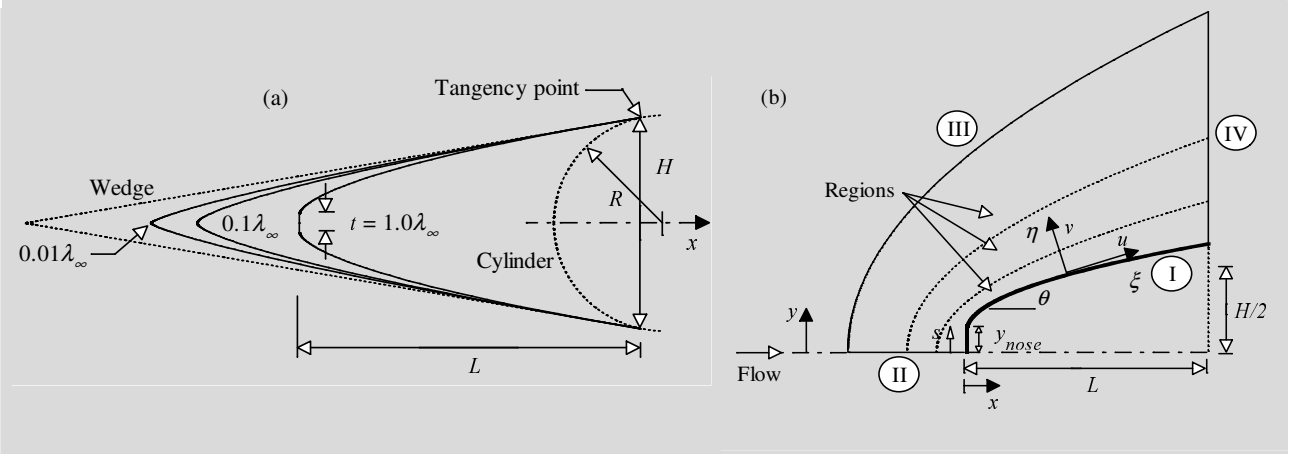

Figure 1: Drawing illustrating (a) the leading edge shapes and (b) the computational domain.

3. Computational Method and Procedure

Navier-Stokes equations, based on the continuum approximation, are adequate to model the fluid behavior for a large class of flows. Continuum approximation implies that the molecular mean free path λ is much smaller than the characteristic length l of interest. It means that the Knudsen number $Kn = \lambda/l << 0.1$. Nevertheless, for a variety of flows, the Knudsen number Kn is of $O(1)$, and the continuum assumption is not valid. In this type of flows, the gas is neither completely in the continuum regime nor in the free molecular flow regime. In this fashion, the flows have been categorized as transitional flows. Examples of such flows are the hypersonic flows about space vehicles or flows in microchannels of microelectro-mechanical (MEMS) devices. In high altitude hypersonic flows, the high Knudsen numbers are mainly due to low density, while in microscale flows the small characteristic length scale results in regions of high Knudsen number, since the flows occur at atmospheric conditions.

Nowadays, the Direct Simulation Monte Carlo (DSMC) method (Bird, 1994), pioneered by Bird in 1960's, has been considered as the most accurate and widely used technique for computation of low density flows. In the DSMC method, the real gas is modeled by thousands or millions of simulated molecules in a computer. The positions, energies and velocity components of the molecules are stored by the computer and are modified over time as the molecules undergo representative intermolecular collisions and boundary interactions in the simulated physical space. Particles that strike the solid wall would reflect according to the appropriate gas-surface interaction model, specular, diffusive or a combination of these. In the collision phase, intermolecular collisions are performed according to the theory of probability without time being consumed. In this context, the intermolecular collisions are uncoupled to the translational molecular motion over the time step used to advance the simulation. Time is advanced in discrete steps such that each step is small in comparison with the mean collision time (Garcia and Wagner, 2000, and Hadjiconstantinou, 2000). All simulations are of an unsteady nature and the time parameter in the simulations may be identified with physical time. For a steady flow problem, the solution is the asymptotic limit of the unsteady flow.

The molecular collisions are modeled using the variable hard sphere (VHS) molecular model (Bird, 1981) and the no time counter (NTC) collision sampling technique (Bird, 1989). The energy exchange between kinetic and internal modes is controlled by the Borgnakke-Larsen statistical model (Borgnakke and Larsen, 1975). Simulations are performed using a non-reacting gas model consisting of two chemical species, N_2 and O_2. Energy exchanges between the translational and internal modes are considered. For a given collision, the probabilities are designated by the inverse of the relaxation numbers, which correspond to the number of collisions necessary, on average, for a molecule to relax. In this simulation, the relaxation number is 5 for rotation and 50 for vibration.

The simulated physical space is divided into an arbitrary number of regions, which are subdivided into computational cells. The cells are further subdivided into four subcells, two subcells/cell in each Coordinate direction. The cell provides a convenient reference sampling of the macroscopic gas properties, whereas the collision partners are selected from the same subcell for the establishment of the collision rate. As a result, the flow resolution is much higher than the cell resolution. The dimensions of the cells must be such that the change in flow properties across each cell is small. The linear dimensions of the cells should be small in comparison with the scale length of the macroscopic flow gradients normal to the streamwise directions, which means that the cell dimensions should be of the order of the local mean free path or even smaller (Alexander et al., 1998 and Alexander et al., 2000).

The computational domain used for the calculation is made large enough so that body disturbances do not reach the upstream and side boundaries, where freestream conditions are specified. A schematic view of the computational domain is depicted in Fig. (1b). According to this figure, side I is defined by the body surface. Diffuse reflection with complete thermal accommodation is the condition applied to this side. In a diffuse reflection, the molecules are reflected equally in all directions, and the final velocity of the molecules is randomly assigned according to a half-range Maxwellian distribution determined by the wall temperature. Advantage of the flow symmetry is taken into account, and molecular simulation is applied to one-half of a full configuration. Thus, side II is a plane of symmetry. In such a boundary, all flow gradients normal to the plane are zero. At the molecular level, this plane is equivalent to a specular reflecting boundary. Side III is the freestream side through which simulated molecules enter and exit. Finally, the flow at the downstream outflow boundary, side IV, is predominantly supersonic and vacuum condition is specified (Guo and Liaw, 2001). At this boundary, simulated molecules can only exit.

Numerical accuracy in DSMC method depends on the grid resolution chosen as well as the number of particles per computational cell. Both effects were investigated to determine the number of cells and the number of particles required to achieve grid independence solutions. Grid independence was tested by running the calculations with half and double the number of cells in ξ and η directions (see Fig. (1b)) compared to a standard grid. Solutions (not shown) were near identical for all grids used and were considered fully grid independent.

4. Computational Conditions

The freestream and flow conditions used in the present calculations are those given by Santos (2003) and summarized in Tab. (1). The gas properties considered in the simulation are those given by Bird (1994) and tabulated in Tab. (2).

In order to simulate the compressibility effects, the freestream velocity V_∞ was assumed to be constant at 1.49, 2.38 and 3.56 km/s, which correspond to freestream Mach number M_∞ of 5, 8, and 12, respectively. The temperature T_w on the leading-edge surfaces is assumed constant at 880 K, which corresponds to 4 times the freestream temperature T_∞. This temperature is chosen to be representative of the surface temperature near the stagnation point.

Table 1: Freestream Conditions

Temperature T_∞ (K)	Pressure p_∞ (N/m^2)	Density ρ_∞ (kg/m^3)	Number density n_∞ (m^{-3})	Viscosity μ_∞ (Ns/m^2)	Mean free path λ_∞ (m)
220.0	5.582	8.753×10^{-5}	1.8209×10^{21}	1.455×10^{-5}	9.03×10^{-4}

Table 2: Gas Properties

	Mole fraction X	Molecular mass m (kg)	Molecular diameter d (m)	Viscosity Index ω
O_2	0.237	5.312×10^{-26}	4.01×10^{-10}	0.77
N_2	0.763	4.65×10^{-26}	4.11×10^{-10}	0.74

The overall Knudsen number Kn_t, defined as the ratio of the freestream mean free path λ_∞ to the leading edge thickness t, corresponds to 100, 10 and 1 for leading edge thickness t/λ_∞ of 0.01, 0.1 and 1, respectively. The Reynolds number Re_t covers the range from 0.193 to 19.3, based on conditions in the undisturbed stream with leading edge thickness t as the characteristic length.

5. Computational Results and Discussion

In order to assess the overall performance of the leading edges, this section will discuss and compare differences on the aerodynamic surface quantities due to the compressibility effects. Aerodynamic surface quantities of particular interest in the transition flow regime are number flux, heat transfer rate, wall pressure, wall shear stress and drag.

5.1. Number Flux

The number flux N is calculated by sampling the molecules impinging on the surface by unit time and unit area. The sensitivity of the dimensionless number flux to variations on the leading-edge thickness and on the freestream Mach number is illustrated in Figs. (2a), (2b) and (2c) for leading-edge thicknesses t/λ_∞ of 0.01, 0.1 and 1, which correspond to thickness Knudsen number Kn_t of 100, 10 and 1, respectively. In this set of figures, the dimensionless number flux N_f stands for the number flux N normalized by $n_\infty V_\infty$, where n_∞ is the freestream number density and V_∞ is the freestream velocity. Also, S is the arc length s along the body surface, measured from the stagnation point, normalized by the freestream mean free path λ_∞.

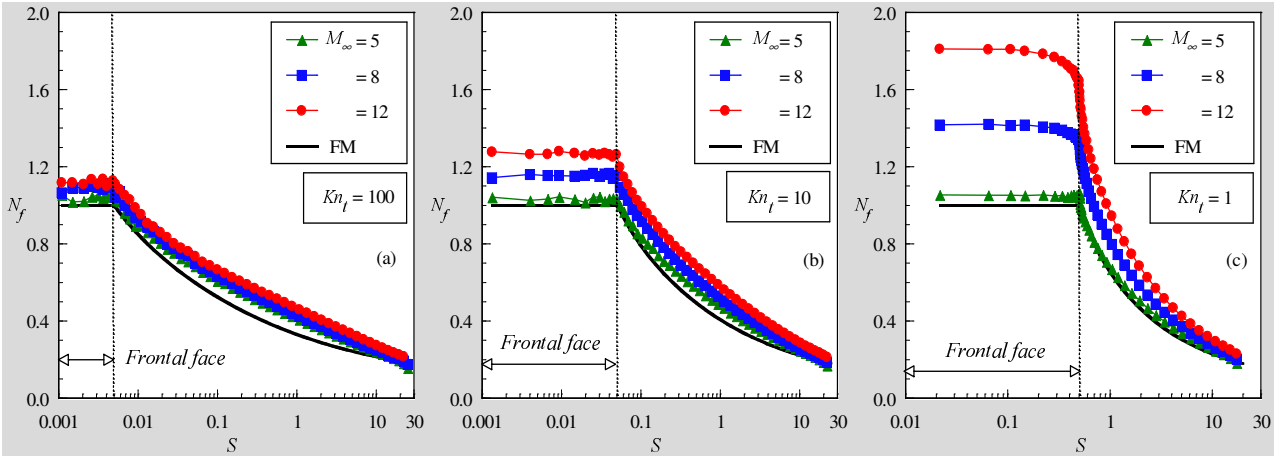

Figure 2: Dimensionless number flux N_f along the body surface as a function of the freestream Mach number for leading-edge thickness corresponding to Knudsen number Kn_t of (a) 100, (b) 10 and (c) 1.

According to these figures, the dimensionless number flux to the surface depends not only on the freestream Mach number but also on the leading-edge thickness. For a sharp leading edge, Kn_t of 100 ($t/\lambda_\infty = 0.01$), the dimensionless number flux is low and constant along the frontal surface and decreases gradually along the afterbody surface. A similar behavior is seen for the slightly blunt leading edge case, Kn_t of 10 ($t/\lambda_\infty = 0.1$). Nevertheless, for the bluntest leading edge case investigated, Kn_t of 1 ($t/\lambda_\infty = 1$), the dimensionless number flux is large on the frontal surface. It presents a constant value along the first half of the frontal face and decreases at the vicinity of the shoulder for the largest freestream Mach number investigated. After that, it decreases significantly along the afterbody surface. The dimensionless number flux rise with increasing the leading-edge thickness may be related to the collisions of two groups of molecules; the molecules reflecting from the body and the molecules oncoming from the freestream. The molecules reflecting from the body surface, which have a lower kinetic energy, interact with the oncoming freestream molecules, which have a higher kinetic energy. Thus, the surface-reflected molecules recollide with the body surface, which produce an increase in the dimensionless number flux in this region. It should be mentioned in this context that,

this behavior is more pronounced with increasing the freestream Mach number, since the molecules oncoming from the freestream have larger kinetic energy. As a result, the net buildup of particle density near the body surface is enhanced.

Free-molecular flow or collisionless flow is the limiting case in which the Knudsen number tends to infinity. It is the subdivision of rarefied gas dynamics corresponding to the lowest densities, therefore with very high mean free paths, or with very small characteristic dimensions. The basic assumption is that intermolecular collisions can be neglected. The fluxes of mass, momentum and energy incident on and reflected from a surface element can be treated separately and do not interfere with each other. The incident flux is entirely unaffected by the presence of the surface. Analytical expressions for number density of the gas just above the surface, number flux, pressure coefficient, heat transfer coefficient and skin friction coefficient have been derived (Bird, 1994) by assuming that the flow past the surface element is in Maxwellian equilibrium with freestream number density n_∞, temperature T_∞, macroscopic velocity V_∞ inclined at an angle of incidence β to the unit normal vector to the surface element, and diffuse reflection. However, the body slope angle θ is related to the angle of incidence β of the element surface by $\pi/2$-β, and it seems to be more appropriate for this work. In this fashion, the number density by considering free molecular flow is given by the following expression,

$$\frac{N}{n_\infty V_\infty} = \frac{1}{2\sqrt{\pi} U_\infty}\left[\exp(-\chi^2) + \sqrt{\pi}\chi(1 + erf\chi)\right] \tag{2}$$

where U_∞ is the speed ratio of the freestream defined by $V_\infty\sqrt{2RT_\infty}$ and $\chi = U_\infty sin\theta$ with R standing for the gas constant.

For comparison purpose, the dimensionless number flux by considering free molecular flow is also displayed in Figs. (2a), (2b) and (2c). It is seen from this set of figures that, for freestream Mach number of 5, the dimensionless number flux along the frontal surface approaches the limit value, $N/n_\infty V_\infty$, = 1, obtained by the Eq. (2). By analyzing Eq. (2), the dimensionless number flux for free molecular flow tends to $sin\theta$ as the freestream speed ratio $U_\infty \to \infty$. As the freestream Mach number increases from 5 to 12, the freestream speed ratio increases from 4.18 to 9.44. As the slope angle θ is 90 degrees for the frontal surface, then the dimensionless number flux becomes independent of the freestream speed ratio or freestream Mach number for free molecular flow.

5.2. Heat Transfer Coefficient

The heat transfer coefficient C_h is defined as being,

$$C_h = \frac{q_w}{\frac{1}{2}\rho_\infty V_\infty^3} \tag{3}$$

where q_w is the net heat flux to the body surface and ρ_∞ is the freestream density.

The heat flux q_w to the body surface is calculated by the net energy flux of the molecules impinging on the surface. A flux is regarded as positive if it is directed toward the surface. The net heat flux q_w is related to the sum of the translational, rotational and vibrational energies of both incident and reflected molecules as defined by,

$$q_w = q_i + q_r = \sum_{j=1}^{N}\left\{\left[\frac{1}{2}m_j v_j^2 + e_{Rj} + e_{Vj}\right]_i + \left[\frac{1}{2}m_j v_j^2 + e_{Rj} + e_{Vj}\right]_r\right\} \tag{4}$$

where N is the number of molecules colliding with the surface by unit time and unit area, m is the mass of the molecules, v is the velocity of the molecules, e_R and e_V stand for the rotational and vibrational energies, respectively. Subscripts i and r refer to incident and reflected molecules.

Distribution of heat transfer coefficient C_h along the body surface is displayed in Figs. (3a), (3b) and (3c) for thickness Knudsen numbers Kn_t of 100, 10 and 1, respectively, and parameterized by the freestream Mach number. It is observed from Fig. (3a) to Fig. (3c) that the heat transfer coefficient is sensitive to the leading-edge thickness as well as to the freestream Mach number. The heat transfer coefficient remains essentially constant over the first half of the frontal surface, and then it decreases sharply and continues to decline along the afterbody surface. However, for the bluntest case investigated, Kn_t = 1 (t/λ_∞ = 1), the heat transfer coefficient increases at the vicinity of the flat-face/afterbody junction, in contrast to the sharpest case investigated, Kn_t = 100. As would be expected, the blunter the leading edge is the lower the heat transfer coefficient at the stagnation point. Moreover, the higher the freestream Mach number the larger the heat transfer coefficient along the frontal surface and at the vicinity of the stagnation region. For the purpose of reference, the heat transfer coefficient at the stagnation point for shapes represented by Kn_t = 100, 10 and 1 at M_∞ = 12 corresponds, respectively, to 2.1, 2.2 and 2.6 times the heat transfer coefficient for the same shapes at M_∞ = 5.

As the freestream Mach number increases from 5 to 12, the kinetic energy of the freestream molecules increases.

As a result, the heat flux to the body surface increases. An understanding of this behavior can be gained by Eq. (4). The incident component of the velocity v of the molecules is a function of the freestream Mach number. However, the reflected component of the molecular velocity is not a function of the freestream Mach number. Due to the diffuse reflection model, the reflected component of the molecular velocity is obtained from a Maxwellian distribution that only takes into account for the temperature of the body surface, which has the same value for the freestream Mach number cases investigated. It should also be emphasized that the number of molecules colliding with the surface by unit time and unit area, N, which appears in Eq. (4), is the same for the incident and reflected components of the heat transfer coefficient C_h. Nevertheless, N dramatically increases on the front surface of the leading edges with increasing the freestream Mach number as shown from Fig. (2a) to Fig. (2c).

Of particular interest in Fig. (3c) is the behavior of the heat transfer coefficient at the vicinity of the flat-face/afterbody junction. As the number of molecules impinging on the body surface decreases (see Fig. (2c)) at the vicinity of the leading edge shoulder, then the velocity of the molecules increases in this region in order to increase the heat transfer coefficient in this region, based on Eq. (4). It should be mentioned in this context that the increase on the molecular velocity in this region is expected due to the flow expansion along the shoulder of the leading edges.

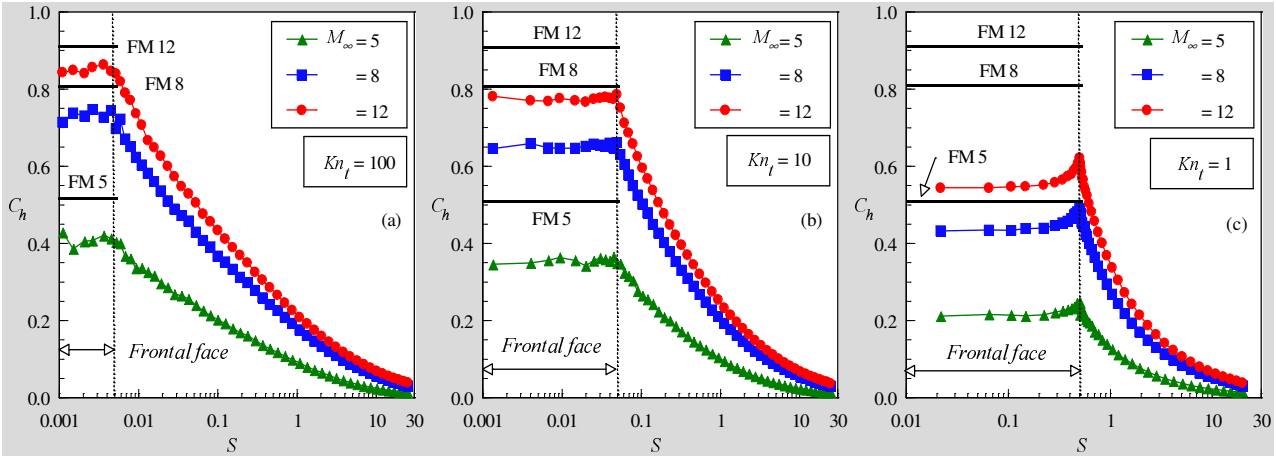

Figure 3: Heat transfer coefficient C_h along the body surface as a function of the freestream Mach number for leading-edge thickness corresponding to Knudsen number Kn_t of (a) 100, (b) 10 and (c) 1.

For completeness, the computations on heat transfer coefficient discussed above are compared to those by considering free molecular flow. The analytical expression (Bird, 1994) for the heat transfer coefficient is given as follows,

$$C_h = \frac{1}{2\sqrt{\pi}U_\infty^3}\left\{\left[U_\infty^2 + \frac{\gamma}{\gamma-1} - \frac{\gamma+1}{2(\gamma-1)}\frac{T_w}{T_\infty}\right]\left[\exp(-\chi^2) + \sqrt{\pi}\chi(1+erf\chi)\right] - \frac{1}{2}\exp(-\chi^2)\right\} \tag{5}$$

where γ specific heat ratio.

By considering free molecular flow, the heat transfer coefficient along the frontal surface, based on Eq. (5), is 0.514, 0.810 and 0.916 for freestream Mach number of 5, 8 and 12, respectively. For purpose of reference, these limit values (FM) are shown in Figs. (3a), (3b) and (3c). It is noticed from these figures that the heat transfer coefficients for the sharpest leading edge investigated, $t/\lambda_\infty = 0.01$, approach those values obtained by considering free molecular flow. As matter of fact, this is an expected behavior since this leading edge corresponds to a thickness Knudsen number Kn_t of 100. In contrast, the flow is far from the free molecular limit for the bluntest leading edge, Kn_t of 1, as shown in Fig. (3c).

5.3. Pressure Coefficient

The pressure coefficient C_p is defined as being,

$$C_p = \frac{p_w - p_\infty}{\frac{1}{2}\rho_\infty V_\infty^2} = \frac{p_w/p_\infty - 1}{\frac{1}{2}\gamma M_\infty^2} = \frac{p_w/p_\infty - 1}{U_\infty^2} \tag{6}$$

where p_w is the pressure acting on the body surface and p_∞ is the freestream pressure.

The pressure p_w on the body surface is calculated by the sum of the normal momentum fluxes of both incident and reflected molecules at each time step as follows,

$$p_w = p_i + p_r = \sum_{j=1}^{N} \left\{ \left[m_j v_{\eta j}^2 \right]_i + \left[m_j v_{\eta j}^2 \right]_r \right\} \tag{7}$$

where v_η is the velocity component of the molecules in the normal direction, i.e., η-direction as shown in Fig. (1b).

The effect on pressure coefficient due to variations on the freestream Mach number and on the leading-edge thickness is demonstrated from Fig. (4a) to Fig. (4c) for thickness Knudsen number Kn_t of 100, 10 and 1, respectively.

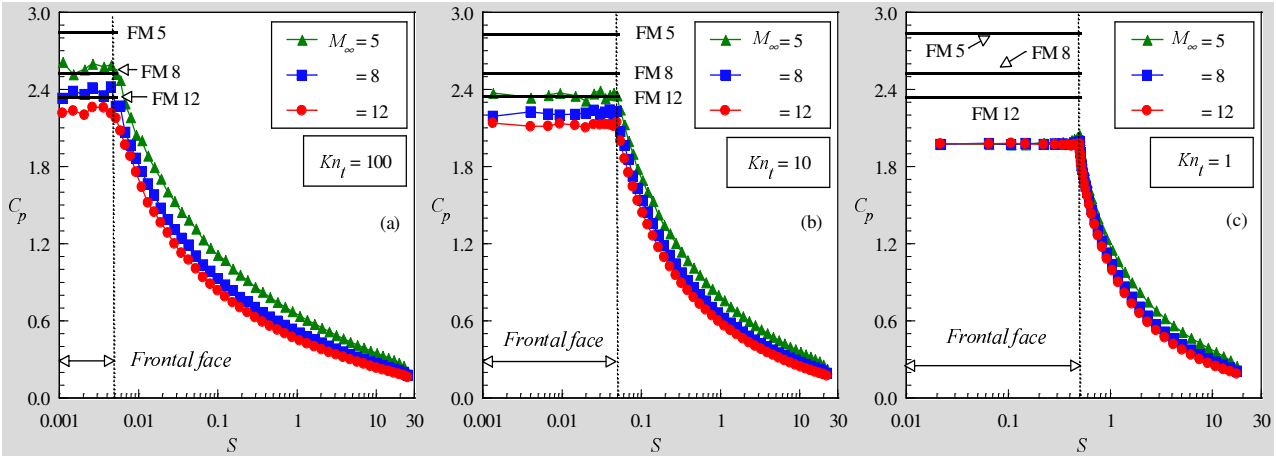

Figure 4: Pressure coefficient C_p along the body surface as a function of the freestream Mach number for leading-edge thickness corresponding to Knudsen number Kn_t of (a) 100, (b) 10 and (c) 1.

Referring to Figs. (4a), (4b) and (4c), it is noted that the pressure coefficient basically present a constant value along the frontal surface and the constant value increases with increasing the freestream Mach number. Subsequently, the pressure coefficient decreases dramatically along the afterbody surface for the cases investigated. In addition, it is clearly noticed in Fig. (4c) that the freestream Mach number rise investigated has no expressive effect on the pressure coefficient for the bluntest leading edge, Kn_t = 1. At this point, it is important to recognize from the number flux distribution in Fig. (2) that significant changes in the number flux occur due to variations not only on the leading edge thickness but also on the wall temperature.

Plotted along with the computational solutions for pressure coefficient is the pressure coefficient limit predicted by the free molecular flow. These values, obtained from Eq. (8) are 2.85, 2.53 and 2.35 for freestream Mach number of 5, 8 and 12, respectively. As expected, the pressure coefficient along the frontal surface for the Kn_t = 100 case approaches the free molecular limit, as shown in Fig. (4a).

$$C_p = \frac{1}{U_\infty{}^2} \left\{ \left[\frac{\chi}{\sqrt{\pi}} + \frac{1}{2} \left(\frac{T_w}{T_\infty} \right)^{1/2} \right] \exp\left(-\chi^2\right) + \left[\frac{1}{2} + \chi^2 + \frac{1}{2} \left(\frac{T_w}{T_\infty} \right)^{1/2} \sqrt{\pi}\chi \right] \left[1 + erf\chi \right] - 1 \right\} \tag{8}$$

Before proceeding with the discussion in this paper, care must be taken with the pressure coefficient changes due to the compressibility effects. The pressure coefficient rise, observed in Figs. (4a) and (4b) as the freestream Mach number decreases, are not associated to a pressure rise on the wall. Equations (6) and (7) provide the necessary assistance in order to understand this behavior. As the freestream Mach number decreases from 12 to 5, the number of particles impinging on the body surface diminishes, as shown in Figs. (2a-c). As a result, the wall pressure, given by Eq. (7), also diminishes. Thus, the numerator of Eq. (6) grows progressively less while the denominator ($\propto M_\infty{}^2$) decreases faster than the numerator and results in a pressure coefficient rise, as shown in Figs. (4a-c).

In what follows, for convenience, the sensitivity of the wall pressure to variations on the freestream Mach number is demonstrated in Figs. (5a), (5b) and (5c) for thickness Knudsen number Kn_t of 100, 10 and 1, respectively. In this set of figures, the wall pressure p_w is normalized by the freestream pressure p_∞. It is noted that the pressure basically present a constant value along the frontal surface and the constant value increases with increasing the freestream Mach number. It can also be seen that the front surface experiences a remarkable pressure compared to the freestream pressure; it is one order of magnitude larger than the freestream pressure for those simulations with M_∞ = 5, and two orders of magnitude larger than the freestream pressure for the other two freestream Mach number cases investigated. It should be mentioned in this context that the large amount of kinetic energy presented in a hypersonic freestream is converted by molecular collisions into high thermal energy surrounding the body and by flow work into increased pressure. In this way, the region at the vicinity of the front surface is a zone of strong compression.

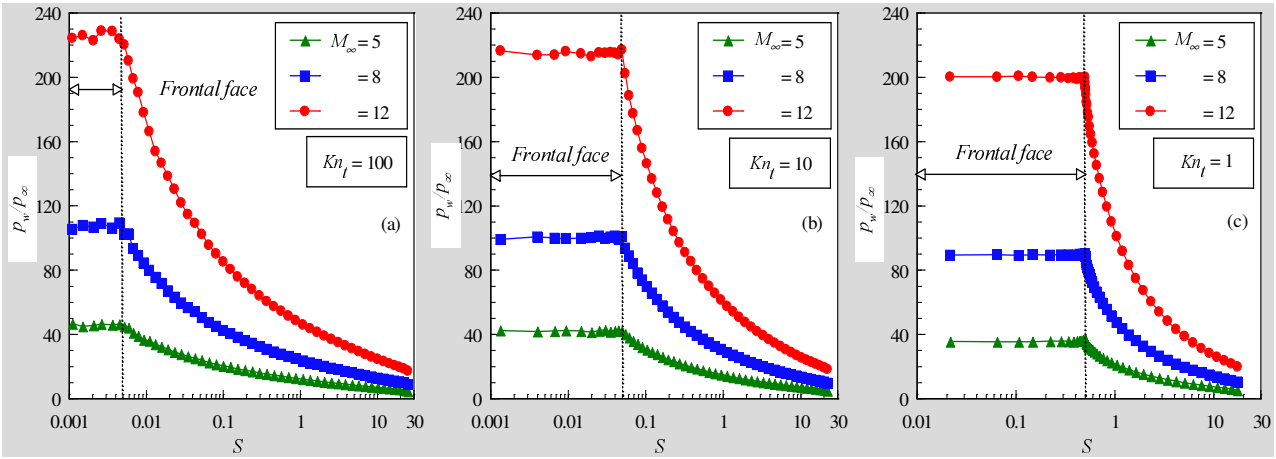

Figure 5: Pressure ratio (p_w/p_∞) along the body surface as a function of the freestream Mach number for leading-edge thickness corresponding to Knudsen number Kn_t of (a) 100, (b) 10 and (c) 1.

5.4. Skin Friction Coefficient

The skin friction coefficient C_f is defined as being,

$$C_f = \frac{\tau_w}{\frac{1}{2}\rho_\infty V_\infty^2} = \frac{\tau_w / p_\infty}{\frac{1}{2}\gamma M_\infty^2} = \frac{\tau_w / p_\infty}{U_\infty^2} \tag{9}$$

where τ_w is the shear stress acting on the body surface.

The shear stress τ_w on the body surface is calculated by averaging the tangential momentum transfer of the molecules impinging on the surface. For the diffuse reflection model imposed for the gas-surface interaction, reflected molecules have a tangential moment equal to zero, since the molecules essentially lose, on average, their tangential velocity component. In this context, the tangential momentum flux of the incident molecules is defined as follows,

$$\tau_w = \sum_{j=1}^{N} m_j v_{\xi j}^2 \tag{10}$$

where v_ξ is the velocity component of the molecules in the tangential direction, i.e., ξ-direction as shown in Fig. (1b).

The variation of skin friction coefficient C_f with the freestream Mach number is depicted from Figs. (6a) to (6c) for Kn_t of 100, 10 and 1, respectively. It is noted that the skin friction coefficient is zero at the stagnation point and slightly increases along the frontal surface up to the flat-face/afterbody junction of the leading edges. After that, it increases dramatically to a maximum value that depends on the leading-edge thickness, and decreases downstream along the afterbody surface. Smaller thickness t (larger Kn_t) leads to higher peak value for the skin friction coefficient. Also, smaller thickness t displaces the peak value to near the flat-face/afterbody junction.

The compressibility effect on the skin friction coefficient can also be seen in a different way by comparing the DSMC computational results along the body surface with that calculated by assuming free molecular flow. For comparison purpose, the skin friction coefficient predicted by the free molecular flow, Eq. (11), is also displayed in Figs. (6a-c).

$$C_f = \frac{\cos\chi}{\sqrt{\pi} U_\infty}\left[\exp(-\chi^2) + \sqrt{\pi}\chi(1 + erf\chi)\right] \tag{11}$$

The skin friction coefficient presents interesting features as it is plotted as a function of the body slope angle θ. Figures (7a), (7b) and (7c) illustrate these features for thickness Knudsen number Kn_t of 100, 10 and 1, respectively. In addition, this set of diagrams displays the skin friction coefficient by assuming a free molecular flow, as defined by Eq. (11). Also, in these figures, 90 degrees correspond to the station at the flat-face/afterbody junction, and 10 degrees correspond to the tangent point common to all of the shapes as shown in Fig. (1a). As can be seen, the skin friction coefficient predicted by free molecular flow exhibits its maximum value at 45 degrees. From Eq. (11), it is found that the maximum skin friction coefficient occurs at 45 degrees when the speed ratio U_∞ is very high, but at zero incidence as the speed ratio U_∞ is extremely small. Similarly, the maximum values for the leading edges obtained by DSMC occur very close to the same station, i.e., 45 degrees.

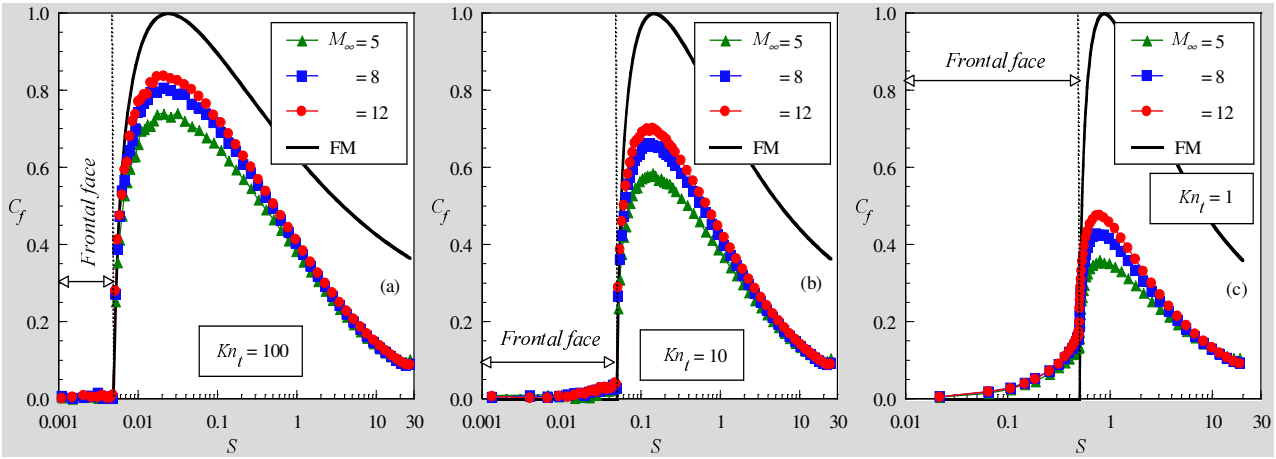

Figure 6: Skin friction coefficient C_f along the body surface as a function of the freestream Mach number for leading-edge thickness corresponding to Knudsen number Kn_t of (a) 100, (b) 10 and (c) 1.

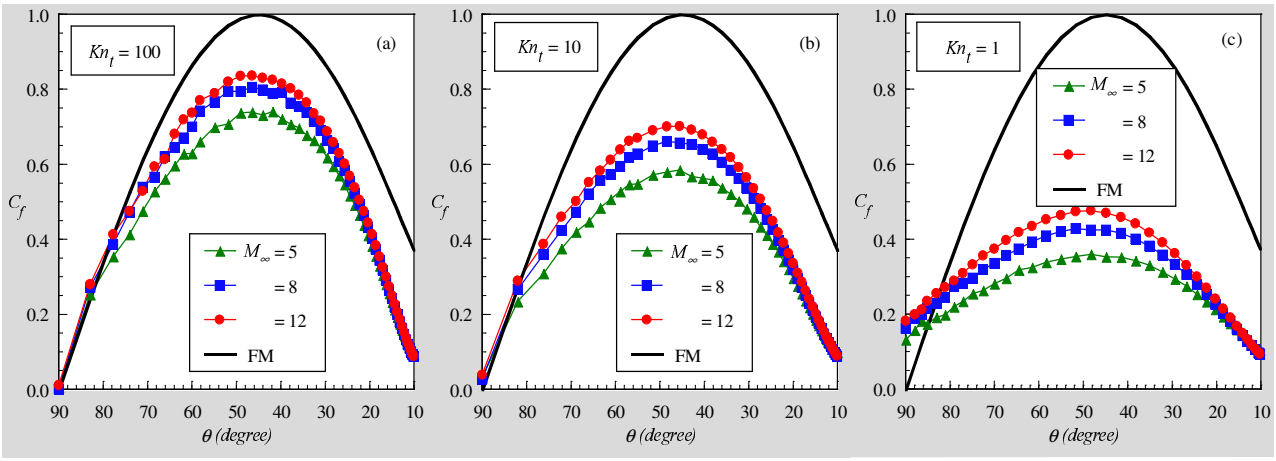

Figure 7: Skin friction coefficient C_f along the afterbody surface as a function of the body slope angle for leading-edge thickness corresponding to Knudsen number Kn_t of (a) 100, (b) 10 and (c) 1.

5.5. Drag Coefficient

The total drag coefficient C_d is defined as being,

$$C_d = \frac{F}{\frac{1}{2}\rho_\infty V_\infty^2 H} \tag{12}$$

where F is the resultant force acting on the body surface and H is the height at the matching point common to the leading edges (see Fig. (1a)).

The drag force is obtained by the integration of the pressure p_w and shear stress τ_w distributions from the stagnation point of the leading edge to the station L, which corresponds to the tangent point common to all of the body shapes, as shown Fig. (1a). It is important to mention that the values for the total drag presented in this section were obtained by assuming the shapes acting as leading edges. Consequently, no base pressure effects were taken into account on the calculations.

The impact of the compressibility effect on the total drag coefficient C_d is displayed in Figs. (8a), (8b) and (8c) for thickness Knudsen number Kn_t of 100, 10 and 1, respectively. In this set of figures, the contributions of the pressure C_{pd} and skin friction drag C_{fd} to the total drag coefficient are also illustrated. It is apparent from this set of diagrams that as the leading edge becomes blunter, i.e., the nose becomes flatter, the contribution of the pressure drag to the total drag increases and the contribution of the skin friction drag decreases, and the net effect results in a slightly increase in the total drag. It is also seen that the total drag decreases with increasing the freestream Mach number.

As a reference, for freestream Mach number of 5, the pressure drag is 39.5%, 45.7% and 61.3% of the total drag for the leading edges defined by Kn_t of 100, 10 and 1, respectively. Consequently, the skin friction contribution decreases from 60.5% to 39.7% for the same cases. On the other hand, for freestream Mach number of 12, the pressure drag is

28.2%, 34.6% and 53.7% of the total drag for the leading edges defined by Kn_t of 100, 10 and 1, respectively. This behavior appears to be fully explained through the changes in pressure and shear stress shown from Figs. (5) to (8). Note that on the front surface, for the same freestream Mach number, the wall pressure decreases as the leading-edge thickness increases, while it increases on the afterbody surface of leading edges. In contrast, the shear stress basically has no contribution on the frontal surface. However, it decreases on the afterbody surface.

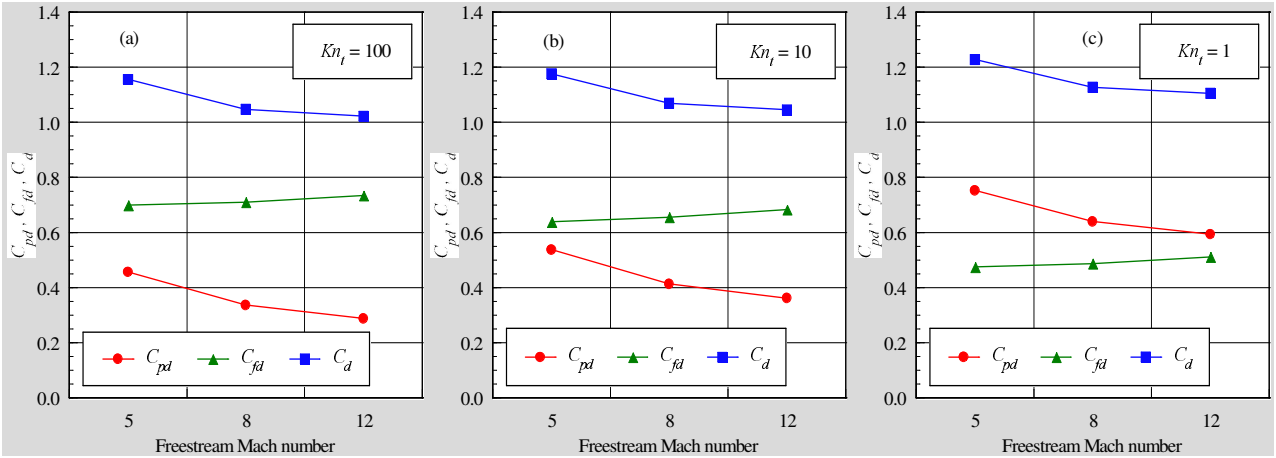

Figure 8: Pressure drag C_{pd}, skin friction drag C_{fd} and total drag coefficient C_d as a function of the freestream Mach number for leading-edge thickness corresponding to Knudsen number Kn_t of (a) 100 and (b) 10 and (c) 1.

For completeness, the total drag coefficient for the cases investigated is tabulated in Tab. (3). Significant differences in the total drag coefficient between freestream Mach number of 5 and 12 are seen on the leading-edge shapes. By referring to Tab.(3), the total drag coefficient for leading edge corresponding to Kn_t of 1decreases around 11% as the freestream Mach number increases from 5 to 12, despite of the fact that the wall pressure and shear stress significantly increase with freestream Mach number, as depicted from Figs. (5) to (8). In order to understand this behavior, Eq. (12) provides the necessary assistance. The numerator of Eq. (12) grows with wall pressure and shear stress, while the denominator ($\propto M_\infty^2$) increases faster than the numerator and results in a total drag coefficient decrease.

Table 3: Total drag coefficient for the flat-nose leading edges.

M_∞	Kn_t = 100	Kn_t = 10	Kn_t = 1
5	1.156	1.176	1.228
8	1.047	1.069	1.127
12	1.022	1.046	1.105

6. Concluding Remarks

The Direct Simulation Monte Carlo method is used to numerically simulate the rarefied hypersonic flow on blunt leading edges. The calculations provided information concerning the nature of the aerodynamic surface quantities for a family of contours composed by a flat nose followed by a highly curved afterbody surface. Effects of compressibility on the number flux, heat transfer coefficient, pressure coefficient, skin friction coefficient and total drag coefficient for a wide range of parameters are investigated. The freestream Mach number was varied from 5 to 12. In addition, the leading-edge thicknesses investigated correspond to thickness Knudsen number of 1, 10 and 100. These cases cover the hypersonic flow from the transition regime to the free molecular one.

Performance results for leading-edge thickness corresponding to thickness Knudsen number of 100 indicated that the aerodynamic surface quantities approach those values predicted by the free molecular flow equations on the frontal surface for the flow conditions considered. Calculations showed that the heat transfer coefficient decreases with increasing the frontal surface of the leading edges, since the leading edge changes from a sharp leading edge to a blunt one. It was found that the heat transfer coefficient increases with the freestream Mach number rise. The analysis also showed that the total drag slightly increases by increasing the leading-edge thickness, and decreases with increasing the freestream Mach number, as would be expected.

7. References

Alexander, F. J., Garcia, A. L., and, Alder, B. J., 1998, "Cell Size Dependence of Transport Coefficient in Stochastic Particle Algorithms", Physics of Fluids, Vol. 10, No. 6, pp. 1540-1542.

Alexander, F. J., Garcia, A. L., and, Alder, B. J., 2000, "Erratum: Cell Size Dependence of Transport Coefficient is Stochastic Particle Algorithms", Physics of Fluids, Vol. 12, No. 3, pp. 731-731.

Bird, G. A., 1981, "Monte Carlo Simulation in an Engineering Context", Progress in Astronautics and Aeronautics: Rarefied gas Dynamics, Ed. Sam S. Fisher, Vol. 74, part I, AIAA New York, pp. 239-255.

Bird, G. A., 1989, "Perception of Numerical Method in Rarefied Gasdynamics", Rarefied gas Dynamics: Theoretical and Computational Techniques, Eds. E. P. Muntz, and D. P. Weaver and D. H. Capbell, Vol. 118, Progress in Astronautics and Aeronautics, AIAA, New York, pp. 374-395.

Bird, G. A., 1994, "Molecular Gas Dynamics and the Direct Simulation of Gas Flows", Oxford University Press, Oxford, England, UK.

Borgnakke, C. and Larsen, P. S., 1975, "Statistical Collision Model for Monte Carlo Simulation of Polyatomic Gas Mixture", Journal of computational Physics, Vol. 18, No. 4, pp. 405-420.

Garcia, A. L., and, Wagner, W., 2000, "Time Step Truncation Error in Direct Simulation Monte Carlo", Physics of Fluids, Vol. 12, No. 10, 2000, pp. 2621-2633.

Guo, K. and Liaw, G.-S., 2001, "A Review: Boundary Conditions for the DSMC Method", Proceedings of the 35th AIAA Thermophysics Conference, AIAA Paper 2001-2953, Anaheim, CA, 11-14 June.

Hadjiconstantinou, N. G., 2000, "Analysis of Discretization in the Direct Simulation Monte Carlo", Physics of Fluids, Vol. 12, No. 10, pp. 2634-2638.

Reller Jr., J. O., 1957, "Heat Transfer to Blunt Nose Shapes with Laminar Boundary Layers at High Supersonic Speeds", NACA RM-A57FO3a.

Santos, W. F. N., 2003, "Aerodynamic Heating on Blunt Nose Shapes in Rarefied Hypersonic Flow", Proceedings of the 17th International Congress of Mechanical Engineering COBEM 2003, 10-14 Nov, São Paulo, SP, Brazil.

Santos, W. F. N., 2004, "Surface Temperature Effects in Low-Density Flow over Flat-Nose Bodies at Hypersonic Speed. Part II: Aerodynamic Suface Quantities", Proceedings of the 10th Brazilian Congress of Thermal Sciences and Engineering ENCIT 2004, 29 Nov – 3 Dec, Rio de Janeiro, RJ, Brazil.

Santos, W. F. N., 2005, "Gas-Surface Interaction Impact on Aerodynamic Surface Quantities of Low-Density Hypersonic Flow over Flat-Nose Bodies", Proceedings of the 18th International Congress of Mechanical Engineering COBEM 2005, 6-11 Dec, Ouro Preto, MG, Brazil.